Nucleic Acids Research, 2024, **52**, 10297–10310
https://doi.org/10.1093/nar/gkae661
Advance access publication date: 1 August 2024
Genome integrity, repair and replication

PHF8 facilitates transcription recovery following DNA double-strand break repair

Jung Eun Kim [1], Xiyue Pan[1], Kwan Yiu Tse[1], Henry Hei Chan[1], Chao Dong[1,2] and Michael Shing Yan Huen [1,*]

[1]School of Biomedical Sciences, LKS Faculty of Medicine, The University of Hong Kong, Hong Kong S.A.R.
[2]Department of Occupational and Environmental Health, School of Public Health, Cheeloo College of Medicine, Shandong University, Jinan, Shandong, China

*To whom correspondence should be addressed. Tel: +852 39176868; Fax: +852 28170857; Email: huen.michael@hku.hk

Abstract

Transient halting of transcription activity on the damaged chromatin facilitates DNA double-strand break (DSB) repair. However, the molecular mechanisms that facilitate transcription recovery following DSB repair remain largely undefined. Notably, failure to restore gene expression in a timely manner can compromise transcriptome signatures and may impose deleterious impacts on cell identity and cell fate. Here, we report PHF8 as the major demethylase that reverses transcriptionally repressive epigenetic modification laid down by the DYRK1B–EHMT2 pathway. We found that PHF8 concentrates at laser-induced DNA damage tracks in a DYRK1B-dependent manner and promotes timely resolution of local H3K9me2 to facilitate the resumption of transcription. Moreover, PHF8 also assists in the recovery of ribosomal DNA (rDNA) transcription following the repair of nucleolar DSBs. Taken together, our findings uncover PHF8 as a key mediator that coordinates transcription activities during the recovery phase of DSB responses.

Graphical abstract

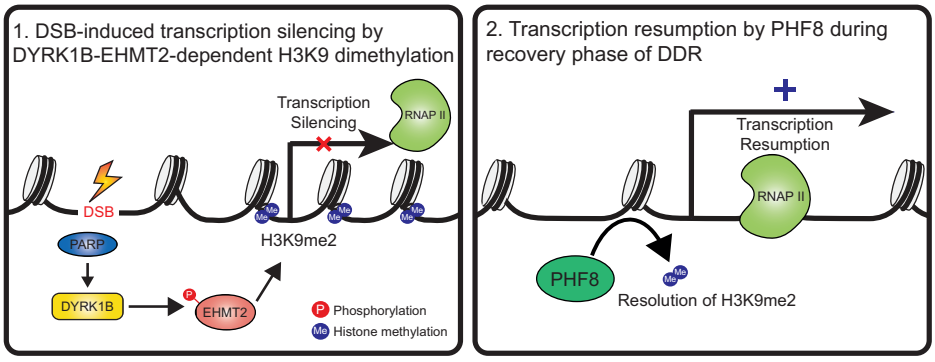

Introduction

DNA double-strand breaks (DSBs) are among the most detrimental types of DNA lesions. Faithful repair of DSBs is crucial for preserving genomic integrity, failing of which may compromise cell proliferation and organismal development. Earlier work has established that cells respond to DSBs by suppressing local transcription activities, an important branch of DNA damage responses (DDRs) that ensures efficient DSB repair by permitting chromatin access to and avoiding clashes with the DNA repair machinery (1,2). Interestingly and counter-intuitively, several lines of evidence suggested that noncoding RNA (ncRNA) molecules are synthesized at sites of DSBs, and that they are important in mounting a full-blown DDR (3). As such, exactly how transcription repression is tempo-spatially coupled to ncRNA production on the damaged chromatin remains to be defined, and warrants further investigations in the distinct transcriptional responses to fully appreciate the mammalian DDR.

The DYRK1B–EHMT2 pathway mediates transcription silencing on chromatin regions surrounding DSBs (4,5), a phenomenon that was termed DSB-Induced Silencing *in Cis* or DISC (6). Briefly, DYRK1B is targeted to DSBs, where it promotes EHMT2 (G9a) phosphorylation and its recruitment to the damaged chromatin. While EHMT2-dependent DISC requires its methyltransferase activity, mechanistically how it temporarily inhibits local transcriptional activity is unclear.

Received: November 13, 2023. **Revised:** July 11, 2024. **Editorial Decision:** July 17, 2024. **Accepted:** July 18, 2024

Given that EHMT2 is endowed with histone methylating activity, and has an established role in catalysing di-methylation of histone H3 at lysine residue 9 (H3K9me2)(7), an established repressive mark associated with gene silencing and formation of heterochromatin (8,9), one would postulate that H3K9me2 may represent an important histone mark that contributes to DISC. Indeed, a scenario has emerged in which histone modifications play active roles in shaping the local chromatin and in orchestrating the many chromatin-templated processes to facilitate DSB repair (1,10).

Notably, although molecular pathways that mediate transcription silencing on the DSB-flanking chromatin domains have been documented, the molecular basis of transcription resumption during DSB repair has remained undefined. One can envisage that a delay in restoring gene expression following DSB repair could perturb the maintenance of transcriptome signatures and may impose a deleterious impact on cell identity and cell fate. Considering that DSB-induced transcription silencing may be effected via local deposition of epigenetic modifications, it is plausible that such chromatin alterations are reversed to drive transcription recovery following DNA repair, although detailed mechanistic bases for cell recovery from genotoxic stress remain unclear.

In line with the role of EHMT2 in catalysing the transcriptionally repressive mark H3K9me2, here we report that DNA damage induces the deposition of H3K9me2 on chromatin-bearing DSBs in a DYRK1B–EHMT2-dependent manner. Further, we found that counteracting H3K9me2 deposition through the ectopic expression of H3K9 demethylases compromised DISC. Building upon these observations, we have identified PHF8 as a key player in resolving H3K9me2 marks on damaged chromatin and in promoting transcription resumption following DSB repair. Together, this study expands our understanding of the regulatory mechanisms of local transcription activity during and after DSB repair, which are essential for maintaining genomic integrity and cellular function.

Materials and methods

Cell culture

U2OS and HEK293T cells were obtained from ATCC. U2OS-DSB reporter cells and U2OS DIvA cells were a generous gift from Roger Greenberg (University of Pennsylvania, Philadelphia, PA) and Gaelle Legube (Université de Toulouse, Toulouse, France), respectively. Cells were cultured in Dulbecco's modified Eagle's medium (DMEM) supplemented with 10% fetal bovine serum (FBS) and 1% penicillin/streptomycin (PS, Gibco, Thermo Fischer Scientific) at 37°C in 5% CO_2.

Plasmids and antibodies

Plasmids and antibodies used for immunofluorescence (IF) staining assays, chromatin immunoprecipitation (ChIP) assays and western blotting in this study are listed in Supplementary Tables S1 and S2, respectively.

Lentivirus packaging and stable cell line generation

To prepare lentiviral particles, lentiviral-based expression plasmids (containing gRNA or expression construct), psPAX2 and pMD2.G were mixed with PEI (Polysciences, #23966) at a 4:3:1 (μg) ratio in DMEM without FBS. After 20 min of incubation at room temperature, the mix was applied to HEK293T cells. The cells were washed with PBS and replaced with fresh DMEM after 8 h of incubation. At 48 and 72 h after transfection, supernatants were collected and passed through a 0.45 μM membrane filter (PALL Life Sciences). The supernatant was mixed with polybrene to a final concentration of 8 μg/ml and was applied to recipient cells. Transduced cells were subjected to antibiotic selection (puromycin, blasticidin S or G418) for the following week, and pooled cells were validated by western blotting. Sequences of gRNAs are listed in Supplementary Table S3.

Small interfering RNA (siRNA)-mediated knockdown

Cells were transfected with non-targeting control or gene-specific siRNAs (Sigma–Aldrich) using Lipofectamine (Invitrogen) twice at 24 h intervals. Samples were collected and subjected to Western blotting to evaluate knockdown efficiency. Sequences of siRNAs are listed in Supplementary Table S4.

FokI-induced DSB generation assay using U2OS-DSB reporter cells

U2OS-DSB reporter cells grown on coverslips were treated with 4-hydroxytamoxifen (4-OHT) and Shield-1 to induce clustered double-strand breaks (DSBs). To induce transcription downstream of DSBs, cells were simultaneously treated with doxycycline (Dox). Following a 4-h incubation, cells were fixed, processed for immunostaining, and subjected to immunofluorescence analysis. Cells were transiently transfected with H3K9me2 demethylase plasmid with PEI prior to DSB induction. Experimental controls, including dimethyl sulfoxide (DMSO) and chemical inhibitors of ATM (KU55933), DYRK1B (AZ191) and EHMT2 (UNC0638), were added to cells at the time of DSB induction at a final concentration of 10 μM. To assay transcription recovery, following DSB induction, cells were washed with PBS and treated with IPTG and Dox. The cells were subsequently fixed for immunofluorescence assay.

Laser micro-irradiation and live cell imaging

Laser micro-irradiation experiments were conducted using a Carl Zeiss LSM780 inverted two-photon laser scanning confocal microscope. The output of the two-photon laser with a wavelength of 750 nm was set at 9%. Two photons of 750 nm combined provide the energy equivalent of a single photon of approximately 375 nm wavelength while allowing for better precision. For live cell imaging, cells grown on glass-bottomed confocal dishes (SPL Life Sciences) were transfected with GFP-tagged plasmids using PEI and underwent laser micro-irradiation in a temperature-controlled (37°C) environmental chamber supplied with 5% CO_2. Time-lapse images of live cells were acquired by Zen 2012 (Carl Zeiss) software using a Plan Apochromat 40×/1.4 oil differential interference contrast (DIC) M27 objective. Acquired images were subsequently processed using ImageJ. Relative MFI was calculated as the difference between average fluorescence intensities in the laser micro-irradiated regions and the nearby undamaged regions of the same nucleus, divided by background.

Chromatin immunoprecipitation and quantitative PCR

Cells were first equilibrated at room temperature (RT) for 10 min. Cross-linking was then performed by treating the cells to a final concentration of 1% paraformaldehyde (PFA) for 10 min. The cross-linking reaction was quenched by adding glycine to a final concentration of 0.125 M, and the cells were incubated for an additional 5 min. Following quenching, the cells were washed twice with ice-cold PBS and harvested by scraping. The harvested cells were pelleted by centrifugation and resuspended in 500 μl of ChIP cell lysis buffer [10 mM Tris–HCl, pH 7.5, 10 mM NaCl, 0.5% NP-40 substitute, protease inhibitor cocktail]. The samples were incubated on ice for 15 min, after which the nuclei were pelleted by centrifugation and resuspended in 300 μl of ChIP buffer [50 mM Tris–HCl, pH 8.0, 100 mM NaCl, 10 mM EDTA, 1% Triton X-100, 0.1% sodium deoxycholate, 0.1% SDS, protease inhibitor cocktail]. Chromatin was then sheared using a Diagenode Bioruptor Pico with settings of 30 s on and 30 s off for 10 cycles, repeated three times with 5-min intervals between sets, to obtain DNA fragments of approximately 200–500 bp. The samples were centrifuged at maximum speed to remove debris. A 1% input of each sample was reserved, and the remaining samples were incubated with Magna ChIP Protein A/G Magnetic Beads (Millipore, 16-663) and the indicated antibodies (H3K9me2, γH2AX or IgG) overnight at 4°C with gentle rotation.

The beads were washed sequentially with ice-cold Low Salt Buffer [20 mM Tris–HCl, pH 8.0, 150 mM NaCl, 2 mM EDTA, 1% Triton X-100, 0.1% SDS], High Salt Buffer [20 mM Tris–HCl, pH 8.0, 500 mM NaCl, 2 mM EDTA, 1% Triton X-100, 0.1% SDS], LiCl Buffer [10 mM Tris–HCl, pH 8.0, 0.25 M LiCl, 1 mM EDTA, 1% NP-40 substitute, 1% sodium deoxycholate], and twice with ice-cold TE buffer [10 mM Tris–HCl, pH 8.0, 1 mM EDTA). The DNA was then eluted and de-cross-linked in ChIP elution buffer [50 mM Tris–HCl, pH 7.5, 50 mM NaCl, 5 mM EDTA, 1% SDS] at 65°C overnight. This was followed by a 1-h incubation with RNase A at 37°C, and a subsequent 1-h incubation with Proteinase K at 55°C. After purifying DNA using the MinElute PCR Purification kit (Qiagen, #28006), quantitative PCR (qPCR) was performed using specific primers (Supplementary Table S5) and the iTaq Universal SYBR Green Supermix (Bio-Rad, #172-5124) on the CFX Opus 384 Real-Time System (Bio-Rad). The input samples were used to calculate the fraction of input for each target.

Co-immunoprecipitation

HEK293T cells were co-transfected with 2 μg of an S protein tag-Flag-Streptavidin binding peptide (SFB)-tagged bait protein plasmid and 6 μg of a Myc-tagged test protein plasmid. Harvested cells were resuspended and lysed on ice for 20 min with NETN lysis buffer [100 mM NaCl, 1 mM EDTA, 20 mM Tris–HCl, pH 8.0, and 0.5% NP-40 substitute] to which Benzonase nuclease (ChemCruz) and 1 mM $MgCl_2$ were added. The lysates were centrifuged at maximum speed at 4°C for 10 min to remove debris.

A 1% input of each sample was reserved, and the remaining samples were incubated with Streptavidin-conjugated agarose beads (Streptavidin Sepharose High Performance; GE Healthcare, 17-5113-01), which were washed twice in NETN buffer. The samples were incubated for 4 h at 4°C with gentle rotation. Protein-bound beads were then washed four times with NETN buffer. The samples were subjected to western blot analysis as described in the following section.

Protein extraction and western blot analysis

Harvested cells were resuspended and lysed on ice for 20 min with NETN lysis buffer [100 mM NaCl, 1 mM EDTA, 20 mM Tris–HCl, pH 8.0, and 0.5% NP-40 substitute] to which Benzonase nuclease (ChemCruz) and 1 mM $MgCl_2$ were added. For subsequent Western blotting, whole cell lysates were mixed with sodium dodecyl sulfate (SDS) loading buffer and boiled at 88°C for 15 min. Lysates were separated by polyacrylamide gel electrophoresis (PAGE) at 165 V for 1 h, followed by semi-dry transfer onto methanol-activated polyvinylidene fluoride (PVDF) membranes. After blocking in 3% skim milk for 1 h, membranes were incubated with primary antibodies diluted in 3% bovine serum albumin (BSA) in 1× TBST at 4°C overnight. Membranes were then washed and incubated in horseradish peroxidase (HRP)-conjugated secondary antibodies at room temperature for 3 h. Membranes were washed and treated with the chemiluminescent solutions (SuperSignal West Pico PLUS Stable Peroxidase and Luminol/Enhancer solution, Thermo Fisher Scientific). Chemiluminescent blot images were captured using Bio-Rad Chemi-Doc MP Imaging System.

DSB generation on endogenous genes using DSB-Inducible via AsiSI (DIvA) platform

U2OS DIvA cells were treated with 4-OHT and Shield-1 for 3 h to induce the AsiSI endonuclease to generate DSBs in genomic DNA. Subsequently, the cells were washed with PBS and incubated in fresh DMEM to facilitate recovery from the DSBs and the silencing of transcription. After treatment, the cells were harvested, and RNA was extracted for RT-qPCR assay.

rDNA DSB induction by I-PpoI

A U2OS cell line stably expressing I-PpoI endonuclease was generated by lentivirus infection and puromycin selection. I-PpoI has a recognition site of 15 bp located within the 28S coding sequence of the rDNA repeats. To induce I-PpoI-targeted rDNA DSBs, cells were incubated in DMEM mixed with 4-OHT and Shield-1 for 3 h. For the transcription recovery assay, cells were washed with PBS and were incubated in fresh DMEM following rDNA DSB induction. After treatment, cells were fixed and were subjected to immunofluorescence assay, or RNA was harvested for RT-qPCR experimentations.

5-Ethynyl uridine (5-EU) incorporation assay

Nascent transcription at DNA damage sites was assayed using the Click-iT RNA Alexa Fluor 594 Imaging Kit (Thermo Fisher Scientific, C10330). Cells grown on coverslips and subjected to DNA damage (laser micro-irradiation-induced DSB or I-PpoI endonuclease-induced rDNA DSB) were incubated with 5-EU-containing DMEM (1 mM final concentration) for 1 h prior to fixation. 5-EU labelling was carried out following the manufacturer instructions. Cells were then counterstained against γH2AX and DAPI and were subjected to an immunofluorescence assay.

Immunofluorescence staining

Following indicated treatment, cells grown on coverslips underwent two washes with ice-cold PBS, were fixed with 3% paraformaldehyde (PFA) for 30 min and were permeabilized with 0.5% Triton X-100 for 30 s at room temperature. The cells were subsequently incubated in primary and secondary antibodies diluted in 3% BSA for 30 min each. When incubating in secondary antibodies, cells were kept in the dark. 4′,6-Diamidino-2-phenylindole (DAPI) was applied for 10 s to stain the nucleus. In between each step, cells were washed with PBS twice. Coverslips were mounted using a mounting medium (Dako, Agilent), and immunofluorescent images were acquired by an Olympus BX51 fluorescence microscope equipped with a UPlanSApo 40×/0.95 objective. The images were analysed using ImageJ software.

RNA isolation and RT-qPCR

RNA extraction was performed with the Quick-RNATM MiniPrep kit (Zymo Research, R1054) following the manufacturer instructions. The reverse transcription (RT) reaction was performed using 1 μg of RNA and SuperScript II Reverse Transcriptase (Invitrogen, #18065-014). The cDNA product from the RT reaction was diluted and was mixed with respective primers (Supplementary Table S6) before being subjected to real-time PCR using the iTaq Universal SYBR Green Supermix (Bio-Rad, #172-5124) on the CFX96 Real-Time System (Bio-Rad). The Cq values were further processed by the $2^{-\Delta\Delta CT}$ method, and GAPDH was used as the internal reference gene.

Statistical analysis

Unless specified otherwise, all data are reported as mean ± SEM from three independent experiments. A two-tailed Student's *t*-test or two-way ANOVA was used for statistical analysis as appropriate, and statistical significance was determined by $P < 0.05$. The symbols used to indicate statistical significance are as follows: ns (non-significant); $*P < 0.05$; $**P \leq 0.01$; $***P \leq 0.001$; $****P \leq 0.0001$.

Results

H3K9me2 mediates transcription silencing on damaged chromatin

The DYRK1B–EHMT2 axis was previously identified as an effector that mediates transcription silencing *in cis* to DSBs (4). Transcription repression by DYRK1B was accomplished via phosphorylation of the histone methyltransferase EHMT2, which promoted its accumulation on the damaged chromatin. Considering that the methyltransferase inactive mutant (EHMT2 ΔSET) was not able to repress transcription upon DSB induction (4) and that EHMT2 catalyses dimethylation of histone H3 lysine residue 9 (H3K9me2) (7), an established transcriptionally repressive histone mark, we hypothesized that EHMT2 may deposit H3K9me2 marks to mediate transcription silencing on the damaged chromatin. To this end, we examined whether H3K9me2 is detected at laser-induced γH2AX-marked DNA damage tracks. Accordingly, we observed a gradual accumulation of H3K9me2 following DSB induction by laser micro-irradiation (Figure 1A). Pre-treatment of cells with chemical inhibitors that specifically target DYRK1B and EHMT2 activities, respectively, led to a marked reduction of the H3K9me2 signal, indicating that the accumulation of H3K9me2 is dependent on the activity of DYRK1B and EHMT2 (Figure 1B and C). Taken together, these observations suggest that DYRK1B facilitates the recruitment of EHMT2 to DSBs, which in turn catalyses the deposition of H3K9me2 marks on the DSB-flanking chromatin to induce local transcription silencing.

To investigate the effect of H3K9me2 in transcription silencing on DSB-flanking chromatin, we used the U2OS-DSB reporter cell line developed by the Roger Greenberg laboratory (Figure 1D) (6). The chromosomally-integrated reporter transgene allows monitoring of *in situ* transcription and clustered DSB induction. Doxycycline (Dox) treatment induces transcription activities that can be monitored by local YFP-MS2 accumulation, whereas 4-hydroxytamoxifen (4-OHT) and Shield-1 treatment lead to the formation of clustered DSBs at the LacO arrays located upstream of the transcription site by promoting the docking of the estrogen receptor (ER)-fused FokI-mCherry-LacI nuclease. To consolidate the role of H3K9me2 in DISC, we over-expressed three different demethylases, namely PHF8, JMJD1A and JMJD2A, all of which have been reported to demethylate H3K9me2 (Figure 1E) (11–16). We reasoned that ectopic expression of H3K9me2 demethylases would counteract EHTM2-dependent H3K9 methylation and thus compromise DISC. Indeed, overexpression of all three demethylases resulted in a substantial increase in cell fractions that supported the colocalization of mCherry-FokI and YFP-MS2 foci, indicating sustained transcription despite the presence of DSBs in its vicinity (Figure 1F and G). Importantly, this inhibitory effect on transcription suppression was dependent on the enzymatic activities of the H3K9me2 demethylases, as point mutations that inactivate the demethylases did not compromise DISC (11,14,15,17). While it is possible that the above observations may have resulted from non-specific effects arising from protein overexpression, a common feature among the three demethylases whose ectopic expression perturbed DISC was their ability to demethylate H3K9me2. Given that forced expression of H3K9me2 demethylases but not their corresponding inactive mutants suppressed DNA damage-induced H3K9me2 deposition flanking DSBs (Figure 1H), these findings strongly suggest that H3K9me2 plays a pivotal role in mediating transcription silencing on DSB-bearing chromatin.

PHF8 is recruited to DSBs in a DYRK1B-dependent manner

To understand how H3K9me2 is dynamically regulated to support transcription recovery following DSB repair, we hypothesized that the histone demethylase(s) must be targeted to the damaged chromatin. To explore this idea, we first examined whether the demethylases could assemble at laser micro-irradiation-induced DSBs (Figure 2A and B). Interestingly, we observed that GFP-PHF8 and GFP-JMJD2A, but not GFP-JMJD1A, accumulated at the laser-induced DNA damage sites (Figure 2A and B). This suggested that PHF8 and JMJD2A may play direct roles in DNA damage responses, potentially regulating H3K9me2 on damaged chromatin.

To determine whether PHF8 and JMJD2A might participate in the DYRK1B–EHMT2 pathway, we tested whether their accumulation at DNA damage sites depends on DYRK1B and EHMT2. Cells expressing GFP-PHF8 or GFP-JMJD2A pre-treated with chemical inhibitors that target DYRK1B (DYRK1Bi) or EHMT2 (EHMT2i) were

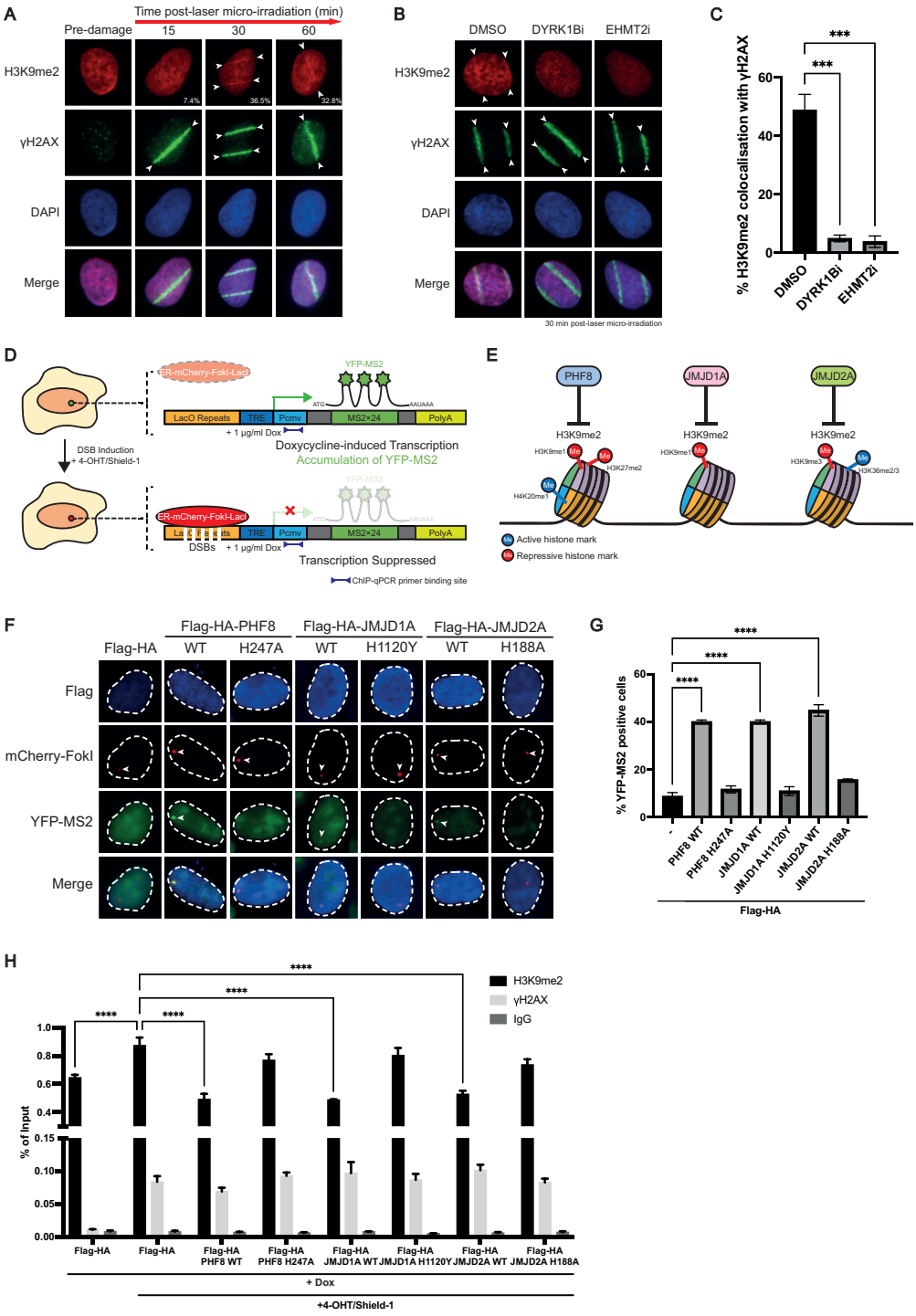

Figure 1. H3K9me2 mediates DSB-induced transcription silencing (**A**) U2OS cells were subjected to laser micro-irradiation stripping. Cells were fixed 15, 30 and 60 min after laser micro-irradiation and processed for immunofluorescence with anti-H3K9me2 and anti-γH2AX antibodies. A gradual accumulation of H3K9me2 at the DSB damage track marked by γH2AX was observed. Quantification shows the percentage of cells with H3K9me2 stripes colocalizing with γH2AX. Arrowheads denote laser micro-irradiated tracks and H3K9me2 stripes. (**B**) U2OS cells were pre-treated with DYRK1B (DYRK1Bi; AZ191) or EHMT2 chemical inhibitor (EHTM2i; UNC0638) for 1 h before laser micro-irradiation. Cells were fixed 30 min after the laser induction and processed for immunofluorescence with anti-H3K9me2 and anti-γH2AX antibodies. Arrowheads denote laser micro-irradiated tracks and H3K9me2 stripes. (**C**) Percentages of cells with H3K9me2 stripes colocalizing with γH2AX were analysed. Bars represent mean ± SEM; $***P \leq 0.001$. (**D**) Schematic illustration of U2OS-DSB reporter system. Doxycycline (Dox) induces transcription and local accumulation of YFP-MS2. 4-hydroxytamoxifen (4-OHT) and Shield-1 induce mCherry-FokI to generate DSBs proximal to the transcription site, leading to suppression of transcription. Blue arrows denote the ChIP-qPCR primer binding site used in (H). (**E**) Schematic illustration of histone demethylases—PHF8, JMJD1A and JMJD2A—utilized in this study and their reported catalytic targets. (**F**) U2OS-DSB reporter cells overexpressing wild type (WT) or catalytically inactive point mutant H3K9me2 demethylases were treated with Dox and 4-OHT/Shield-1. Arrowheads denote mCherry-FokI or YFP-MS2 foci. (**G**) Quantification shows the percentage of YFP-MS2 positive cells. Bars represent mean ± SEM; $****P \leq 0.0001$. (**H**) ChIP-qPCR results show enrichment of H3K9me2 and γH2AX at the transgene before and after FokI-generated DSBs and in cells overexpressing WT or mutant H3K9me2 demethylases. 4-OHT/Shield-1 treatment induces FokI-generated DSBs. IgG was used as a negative control for ChIP. Bars represent mean ± SEM; $****P \leq 0.0001$.

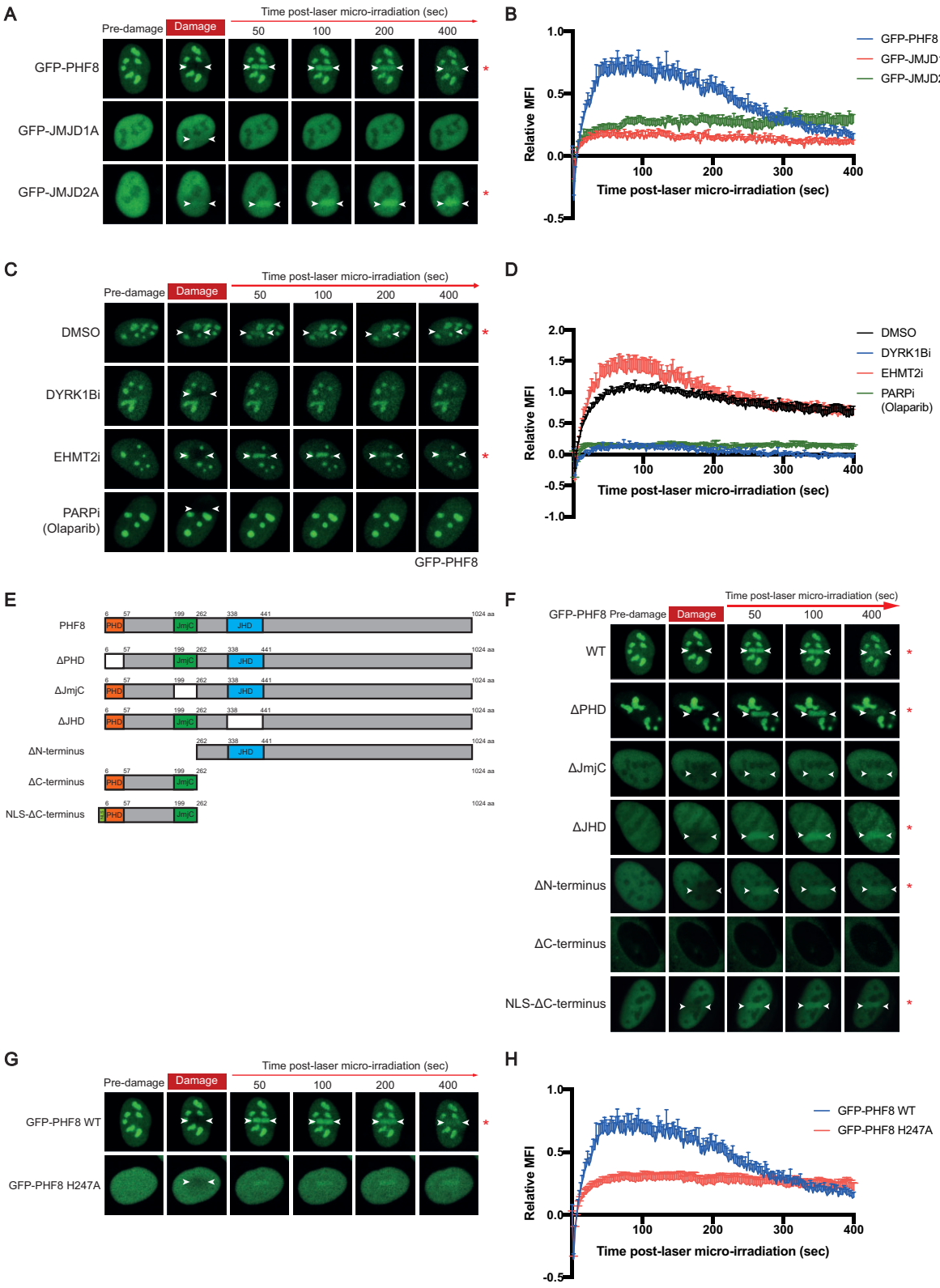

Figure 2. PHF8 dynamics in response to DNA damage. (**A**) U2OS cells transfected with GFP-tagged demethylase expression constructs (GFP-PHF8, GFP-JMJD1A and GFP-JMJD2A) were subjected to laser micro-irradiation. Live cell time-lapse images were taken for analysis of the recruitment. Arrowheads denote laser micro-irradiated tracks. Red asterisks denote the accumulation of GFP-demethylase to the laser-induced track. (**B**) Relative mean fluorescence intensity (MFI) at the laser-induced track was quantified. At least 10 cells from three independent experiments were analysed for each protein. (**C**) U2OS cells transfected with GFP-PHF8 were pre-treated with DYRK1Bi, EHMT2i or PARP inhibitor (PARPi; Olaparib) for 1 h and were subjected to laser micro-irradiation. (**D**) Quantification was processed as described in (B). (**E**) Schematic illustration of PHF8 protein domains and truncated mutants. U2OS cells transfected with GFP-tagged PHF8 wild type (WT) and truncated mutants (ΔPHD, ΔJmjC, ΔJHD, ΔC-terminus, ΔN-terminus and NLS-ΔN-terminus) (**F**) or catalytically inactive point mutant H247A (**G**) were subjected to laser micro-irradiation. (**H**) Quantification was processed as described in (B).

subjected to laser micro-irradiation. While neither DYRK1B nor EHMT2 inhibition affected GFP-JMJD2A accrual at DSBs (Supplementary Figure S1A), we found that DSB association of GFP-PHF8 required DYRK1B but not EHMT2 activity (Figure 2C and D), congruent with our observation that PHF8 complexes with DYRK1B (Supplementary Figure S1B). In addition, PHF8 assembly at laser-induced DSBs was suppressed in cells pre-treated with the PARP inhibitor Olaparib (Figure 2C and D) and the PARP1-specific inhibitor AZD5305 (Supplementary Figure S1C and D). By contrast, cell pre-treatment with PARG inhibitor (PARGi; PDD00017273) led to hyper-accumulation of GFP-PHF8 at laser-induced DNA damage tracks (Supplementary Figure S1C and D). Based on these results, we postulate that PHF8 might participate in the PARP1–DYRK1B–EHMT2 pathway and that, via its putative role in demethylating H3K9me2 marks, it might be responsible for restoring transcription following DSB repair.

To further investigate the requirement for the accumulation of PHF8, we generated a panel of deletion mutants that span the PHF8 polypeptide to identify region(s) responsible for its accumulation at DSBs (Figure 2E). Upon expressing the GFP-tagged PHF8 alleles in U2OS cells, we observed that nucleolar localization of PHF8 relied on its JmjC, JHD and C-terminus, with the C-terminus being critical for its nuclear localization (Figure 2E and F and Supplementary Figure S1E and F). Because the GFP-ΔC-terminus failed to localize to the nucleus, we fused a nuclear localization signal (NLS) sequence to facilitate its nuclear localization in order to determine whether the ΔC-terminus can be recruited to laser-induced DNA damage tracks (Figure 2E and F and Supplementary Figure S1E and F).

We subjected cells expressing GFP-PHF8 alleles to laser micro-irradiation and examined the recruitment patterns of the mutants to the damage sites. Intriguingly, only the JmjC domain deletion mutant (ΔJmjC) displayed a much attenuated ability to localize at DSBs (Figure 2F). To further examine the requirement of PHF8 catalytic activity in its ability to assemble at DSBs, we utilized the PHF8 H247A point mutant, which has been reported to inactivate its demethylase activity (11,18). Consistently, the H247A mutation hampered the recruitment of PHF8 at laser-induced DSBs (Figure 2G and H), suggesting that PHF8 may concentrate on the damaged chromatin in a manner that is regulated by its demethylase activity.

PHF8 resolves DSB-associated H3K9me2 and promotes the resumption of transcription post-DSB repair

Given the established role of PHF8 in demethylating H3K9me2, we then assessed whether PHF8 may promote H3K9me2 resolution on damaged chromatin during cell recovery from DSBs. We subjected PHF8 knockout (KO) cells to laser micro-irradiation, fixed them at time point intervals post-damage, and compared the level of H3K9me2 stripe-positive cells to that of non-targeting (NT) gRNA cells. Accordingly, we found a gradual reduction in H3K9me2 at laser-induced DNA damage tracks in control U2OS cells (Figure 3A–D). By contrast, H3K9me2 marks persisted in PHF8-deficient cells (Figure 3A–C). By contrast, PHF8 inactivation did not noticeably affect the kinetics of H3K9me1, H3K27me2 nor H4K20me1 at laser-induced DNA damage tracks (Supplementary Figure S2A–C). To exclude potential off-target effects arising from PHF8 gRNA and to examine the requirement of its demethylase activity, we reconstituted PHF8-inactivated cells with either wild-type PHF8 or its catalytic inactive H247A mutant. In line with a requirement for its H3K9me2 demethylating activity, wild-type PHF8 but not its H247A allele complemented loss of PHF8 in the timely resolution of H3K9me2 at laser-induced DNA damage tracks (Figure 3A–C). Collectively, this data underlines the role of PHF8 in the timely removal of H3K9me2 marks on the chromatin during cell recovery from DSBs.

To directly assess the role of PHF8 in transcription recovery during DSB responses, we inactivated PHF8 in USO2-DSB reporter cells (Figure 4A and B) and monitored YFP-MS2 foci over a time course. To allow cells to recover from DSBs, following FokI-induced DSBs, we treated cells with IPTG to competitively inhibit mCherry-FokI binding to the LacO repeats, which effectively stops further DSB generation to allow for repair and transcription resumption (Figure 4A). Consistently, we observed fewer cells with YFP-MS2 foci in cases where PHF8 was silenced (Figure 4B–D), further strengthening the role of PHF8 in promoting transcription resumption during cell recovery from DSBs. Moreover, similar to the delayed resolution of H3K9me2 marks at laser-induced DNA damage tracks in PHF8-deficient cells (Figure 3C), H3K9me2 at the artificial transcription reporter, determined by ChIP-qPCR analyses, also persisted following PHF8 inactivation (Figure 4E). Together, these data suggest that PHF8 may target H3K9me2 at DSBs to facilitate timely resumption of transcription during the recovery phase of DDR.

To corroborate a more physiological role of PHF8 in restoring transcription during DSB repair, we borrowed the DIvA (DSB Induced via AsiSI) platform (19), and analysed transcription recovery following induction of genome-wide DSBs by expressing the AsiSI endonuclease. Taking advantage of previous work that has documented transcription repression in proximity to AsiSI-induced DSBs (20), we followed the expression of two genes that have been shown to be repressed in response to AsiSI induction (Figure 5A and B). To this end we generated PHF8-deficient DIvA cell lines (Figure 5C), and determined nascent mRNA expression of GNE and RBMXL1 by RT-qPCR using intron-spanning primers over an 8-h time course following induction and recovery from AsiSI-DSBs. Consistently, we found that PHF8 inactivation resulted in delayed recovery of transcription of both GNE and RBMXL1 (Figure 5D).

PHF8 is dispensable for the repair of IR-induced DSBs

Delay in transcription resumption may also arise as a result of compromised DNA repair. To exclude this possibility, we examined if PHF8 deficiency may affect DSB foci kinetics by challenging cells with a recoverable dose (i.e. 3 Gy) of ionizing radiation (IR). Interestingly, we found that both control cells transduced with NT gRNA and cells transduced with PHF8 gRNA displayed comparable levels of DNA damage markers, including γH2AX, 53BP1, RAD51 and BRCA1 over 16 h after 3 Gy IR exposure (Figure 6A–C). Together with the indistinguishable kinetics of γH2AX at micro-irradiated sites (Figure 3D) and at FokI-induced DSBs (Figure 4E), our observations suggest that PHF8 does not play a major role in DSB repair *per se*.

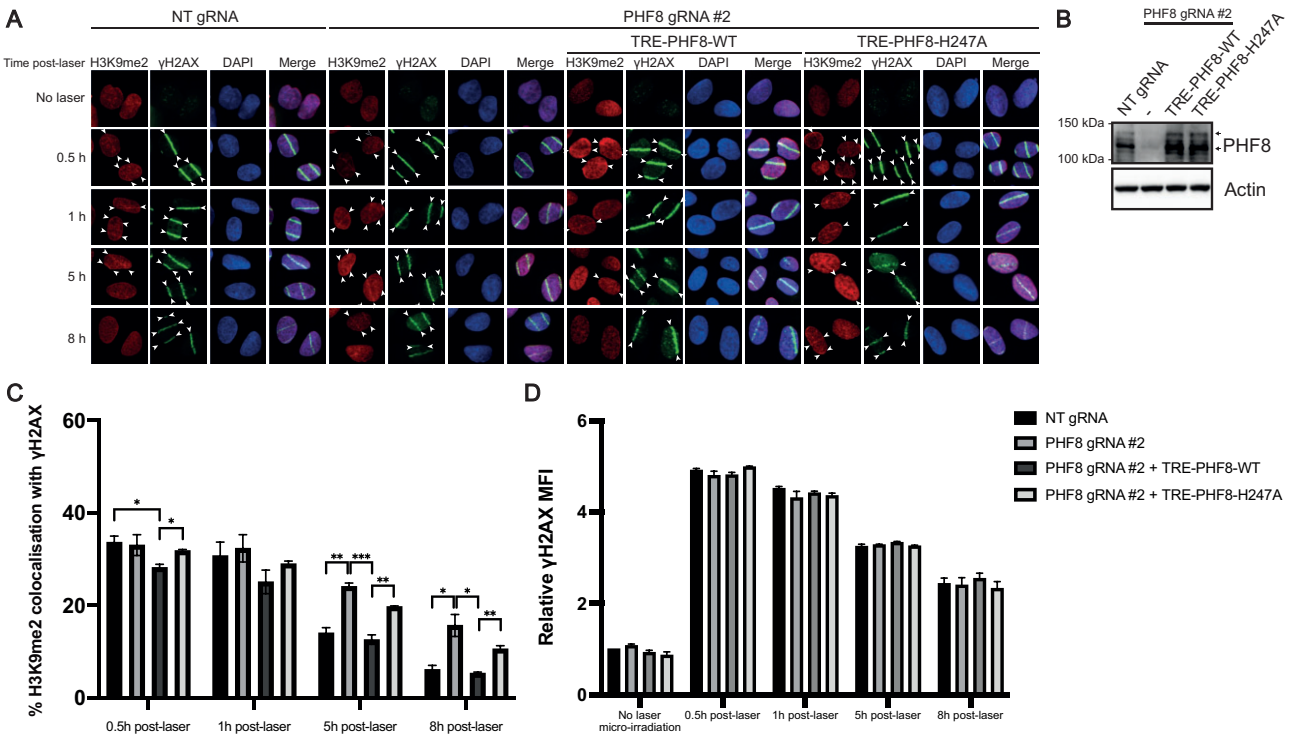

Figure 3. PHF8 promotes H3K9me2 demethylation on damaged chromatin during DSB repair. (**A**) U2OS cells were transduced with non-targeting gRNA (NT gRNA) or PHF8-targeting gRNA (PHF8 gRNA #2). PHF8 gRNA #2 transduced U2OS cells were reconstituted with dox-inducible TRE-PHF8-WT or TRE-PHF8-H247A. After being subjected to laser micro-irradiation stripping, cells were fixed after 30 min, 1 h, 5 h and 8 h and processed for immunofluorescence with anti-H3K9me2 and anti-γH2AX antibodies. Arrowheads denote H3K9me2 stripes or laser micro-irradiated tracks. (**B**) Western blotting was performed to evaluate PHF8 expression. Arrows denote the bands of endogenous PHF8. (**C**) Percentages of cells with H3K9me2 stripes colocalizing with γH2AX were analysed. Bars represent mean ± SEM; $*P < 0.05$; $**P \leq 0.01$; $***P \leq 0.001$. (**D**) Relative γH2AX mean fluorescence intensity was analysed and plotted. Bars represent mean ± SEM.

PHF8 promotes transcription resumption of rRNA synthesis following I-PpoI induction

Given the enrichment of PHF8 in the nucleoli (Supplementary Figure S1E) and its role in promoting transcription recovery following DSB induction (Figures 3–5), and considering that DYRK1B is important in suppressing rDNA transcription following ribosomal DNA (rDNA) damage (5), we examined the possible role of PHF8 in reactivating rDNA transcription following nucleolar DSB repair. To this end, we turned to the I-PpoI endonuclease, which specifically targets rDNA repeats (Figure 7A). In this system, the estrogen receptor-peptide fused-I-PpoI endonuclease generates site-specific DSBs on the 28S sequence of rDNA upon treatment with 4-OHT and Shield-1 (Figure 7A). We transduced U2OS cells stably expressing inducible I-PpoI with lentiviral particles containing PHF8-targeting gRNAs to inactivate PHF8. We treated PHF8-silenced cells with 4-OHT and Shield-1 to induce nuclear translocation of I-PpoI, washed cells with PBS twice and incubated them with fresh medium to allow recovery from rDNA DSBs. To visualize nascent rRNA transcription, we incubated cells with uridine analogue 5-ethynyl uridine (5-EU) for 1 h prior to fixation. The intensity of 5-EU within the nucleolar region was quantified to probe *de novo* RNA synthesis. Upon I-PpoI induction, 5-EU incorporation in the nucleolus was initially suppressed but gradually increased over time following I-PpoI washout, indicating recovery of rRNA transcription (Figure 7B–E). Compared to NT gRNA-transduced cells, PHF8 gRNA-transduced cells showed a slower rate of recovery of 5-EU incorporation post-I-PpoI washout, although no noticeable difference in γH2AX was observed, supporting a role of PHF8 in facilitating transcription resumption following rDNA DSB repair.

To further validate that 5-EU incorporation reflects *de novo* rRNA synthesis, and to substantiate the role of PHF8 in rDNA transcription recovery, we also quantified the expression level of 45s pre-rRNA by reverse transcription-quantitative polymerase chain reaction (RT-qPCR) after I-PpoI induction at different time points (Figure 7F). Consistent with findings derived from the 5-EU incorporation assay, PHF8-inactivated cells exhibited slower recovery in restoring pre-rRNA expression post-I-PpoI washout (Figure 7G and H), which coincided with delayed resolution of DNA damage-induced H3K9me2 at the rDNA repeats (Figure 7I and J). Furthermore, RNA interference (RNAi)-mediated knockdown of PHF8 also led to a delayed recovery in pre-rRNA expression after I-PpoI washout (Supplementary Figure S3A and B). These experiments collectively support the idea that PHF8 facilitates transcription resumption following rDNA DSB repair.

Discussion

In this study, we report that the DYRK1B–EHMT2 pathway promotes H3K9 dimethylation at laser-induced DNA damage tracks and that H3K9me2 represents a histone mark that supports local transcription silencing on DSB-flanking chromatin. Moreover, we also identified PHF8 as a histone-demethylating activity that reverses the H3K9me2 mark during cell recovery from DSBs and that it is important in driving the timely re-

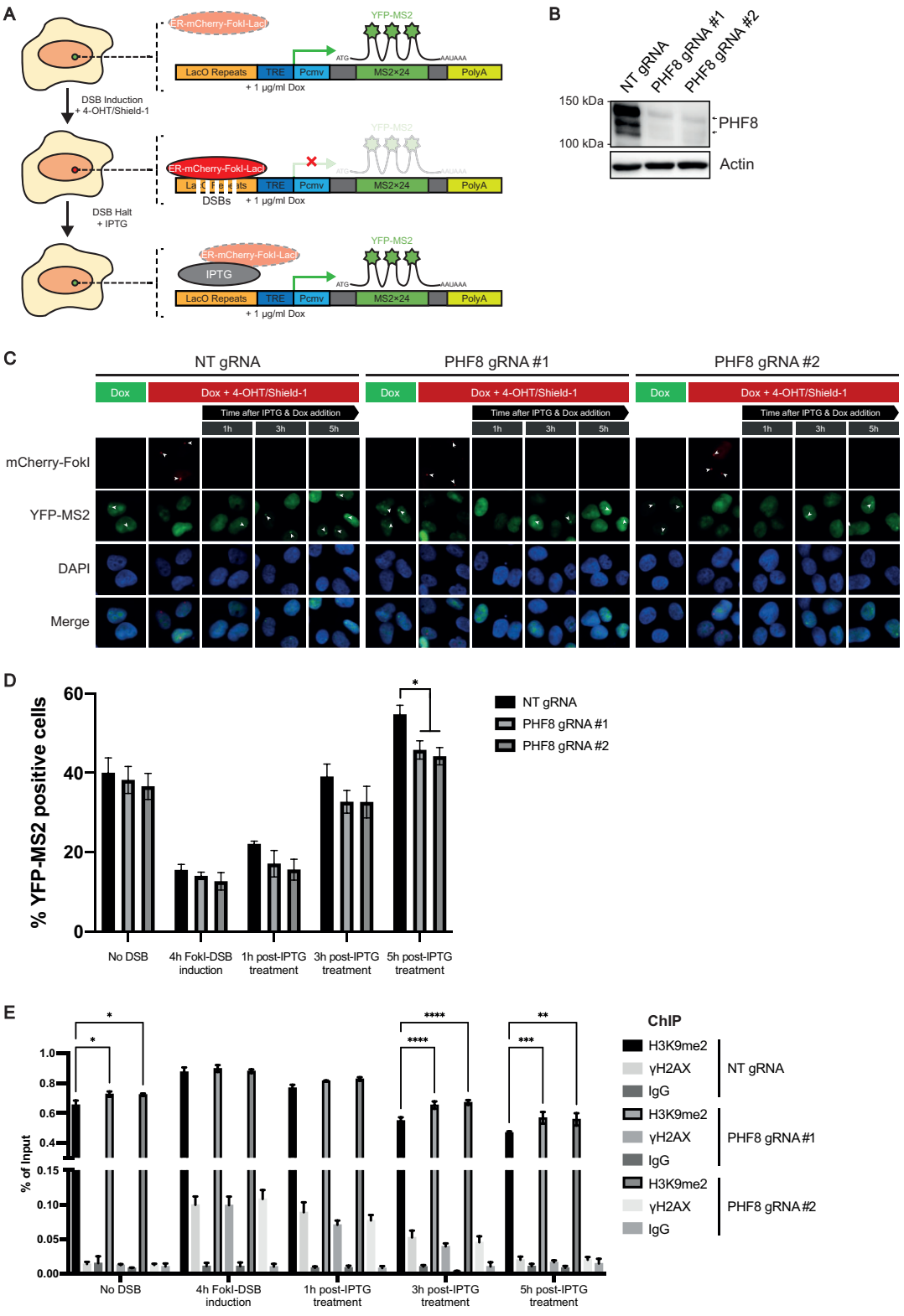

Figure 4. PHF8 promotes timely transcription recovery during DSB repair. (**A**) Schematic illustration of U2OS-DSB reporter system. After DSB induction by treating the cells with 4-OHT and Shield-1, IPTG treatment halts further DSB generations by competitively inhibiting mCherry-FokI from binding to the LacO repeats, thereby allowing for DSB repair and subsequent transcription recovery. (**B**) U2OS-DSB reporter cells were transduced with NT gRNA or PHF8-targeting gRNAs (PHF8 gRNA #1 and PHF8 gRNA #2). Western blotting was performed to evaluate PHF8 expression. Arrows denote the bands of endogenous PHF8. (**C**) U2OS-DSB reporter cells transduced with NT gRNA or PHF8 gRNA #1 or #2 were treated with 4-OHT and Shield-1 to generate FokI-induced DSBs for 4 h. Afterwards, cells were washed with PBS and treated with IPTG to halt the DSBs and allow for repair. Cells were treated with Dox throughout the experiment. Cells were fixed 1, 3 and 5 h after IPTG treatment and processed for immunofluorescence analysis. Arrowheads denote mCherry-FokI or YFP-MS2 foci. (**D**) Quantification shows the percentage of YFP-MS2 positive cells. Bars represent mean ± SEM; $*P < 0.05$. (**E**) ChIP-qPCR results show enrichment of H3K9me2 and γH2AX at different time points in cells transduced with NT gRNA or PHF8 gRNA #1 or #2. IgG was used as a negative control for ChIP. Bars represent mean ± SEM; $*P < 0.05$; $**P \leq 0.01$; $***P \leq 0.001$; $****P \leq 0.0001$.

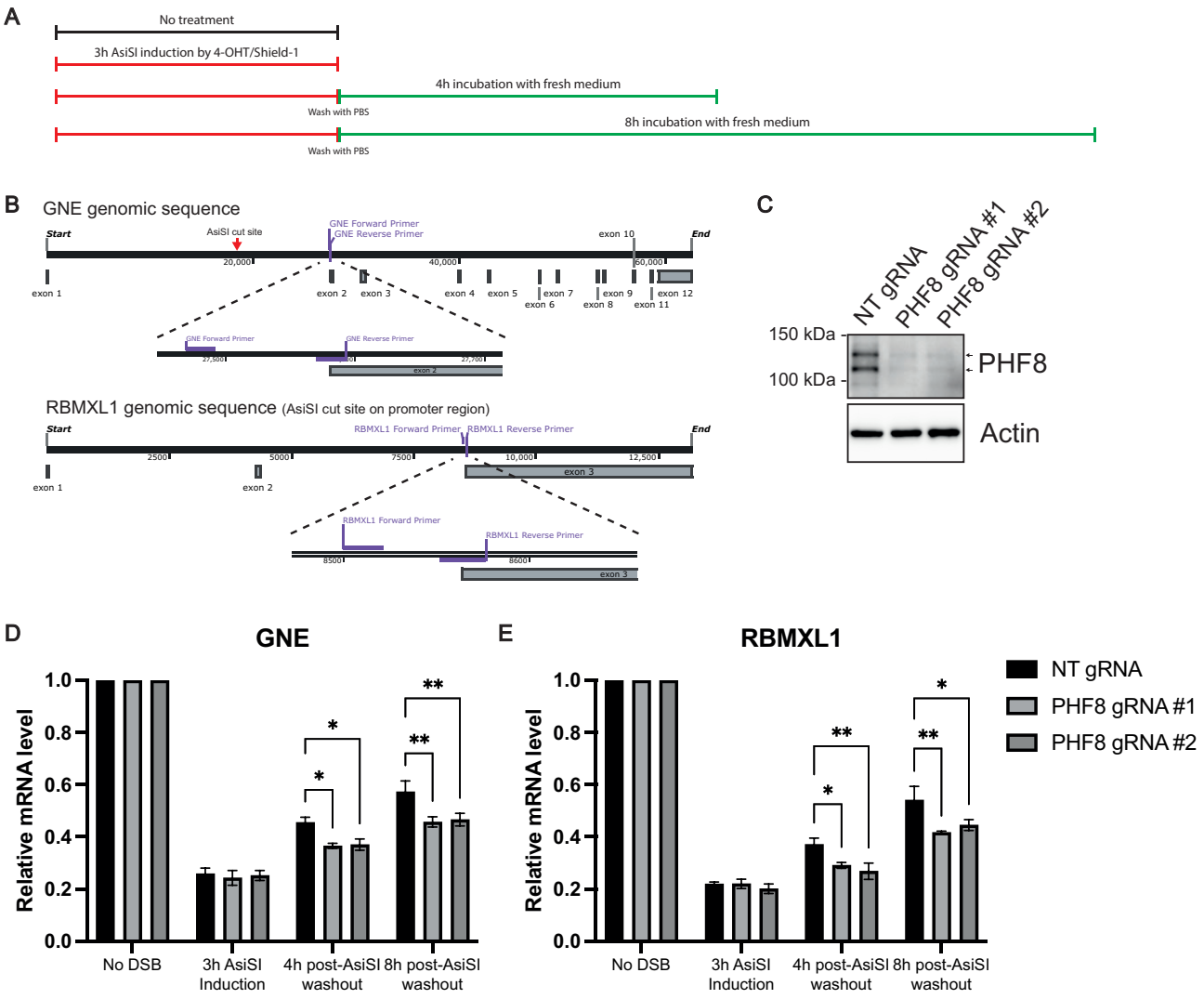

Figure 5. PHF8 promotes transcription recovery of silenced endogenous genes during DSB repair. (**A**) Schematic illustration of the experimental timeline for transcription recovery experiment using the U2OS DIvA cell line. U2OS DIvA cells transduced with NT gRNA or PHF8 gRNA #1 or #2 were treated with 4-OHT and Shield-1 for 3 h to induce AsiSI-generated DSBs at endogenous genes, followed by washing with PBS and incubation with fresh DMEM for 4 h or 8 h to allow for DSB repair and transcription recovery. (**B**) Schematic illustration of the genomic sequences of GNE and RBMXL1, indicating the AsiSI cut sites, exons and intron–exon spanning primers used for RT-qPCR. (**C**) Western blotting was performed to evaluate PHF8 expression. Arrows denote the bands of endogenous PHF8. RT-qPCR analysis of GNE (**D**) or RMBXL1 (**E**) nascent mRNA levels in NT gRNA and PHF8 gRNA transduced U2OS DIvA cells. Each cell group data were normalized to its own No DSB treatment group, respectively. Bars represent mean ± SEM; $*P < 0.05$; $**P \leq 0.01$.

sumption of transcription. Together, these findings provide insights into the dynamic regulation of H3K9me2 on damaged chromatin, entailing an intimate interplay between EHMT2 and PHF8.

While it has been obscure if H3K9me2 may be deposited on the damaged chromatin (21), we have provided several lines of evidence to support the role of H3K9me2 in transcription repression on the DSB-flanking chromatin. Indeed, not only have we identified the DYRK1B–EHMT2 pathway as key to DSB-associated H3K9 dimethylation (Figure 1B and C), we also found that forced expression of H3K9me2 demethylases led to compromised DISC (Figure 1F–H). Given the established role of H3K9me2 in the formation of transcriptionally silent heterochromatin domains (8,9), one would postulate that H3K9me2 on the DSB-flanking chromatin may facilitate DSB repair by first remodelling the damaged chromatin into a condensed state, thereby preventing nearby gene expression that may otherwise interfere with DNA repair processes. As such, we speculated that H3K9me2 kinetics on the damaged chromatin may correlate with the DSB repair status. Indeed, the dynamics of H3K9me2 on damaged chromatin correlated closely with the DNA damage marker γH2AX, and have prompted us to propose that histone demethylase(s) may be involved in the process to reverse the methylation status, thus allowing for resumption of transcription during DSB repair. Our data, therefore, supports the notion that the dynamic interplay between histone-modifying enzymes, including demethylases, is crucial in enabling resumption of transcription following DSB repair.

Contrary to previous literature implicating PHF8 in homologous recombination (HR) and non-homologous end joining (NHEJ) repair (22), our observation suggests that PHF8 deficiency does not noticeably affect the resolution of DSB markers, but instead contributes to transcription resumption

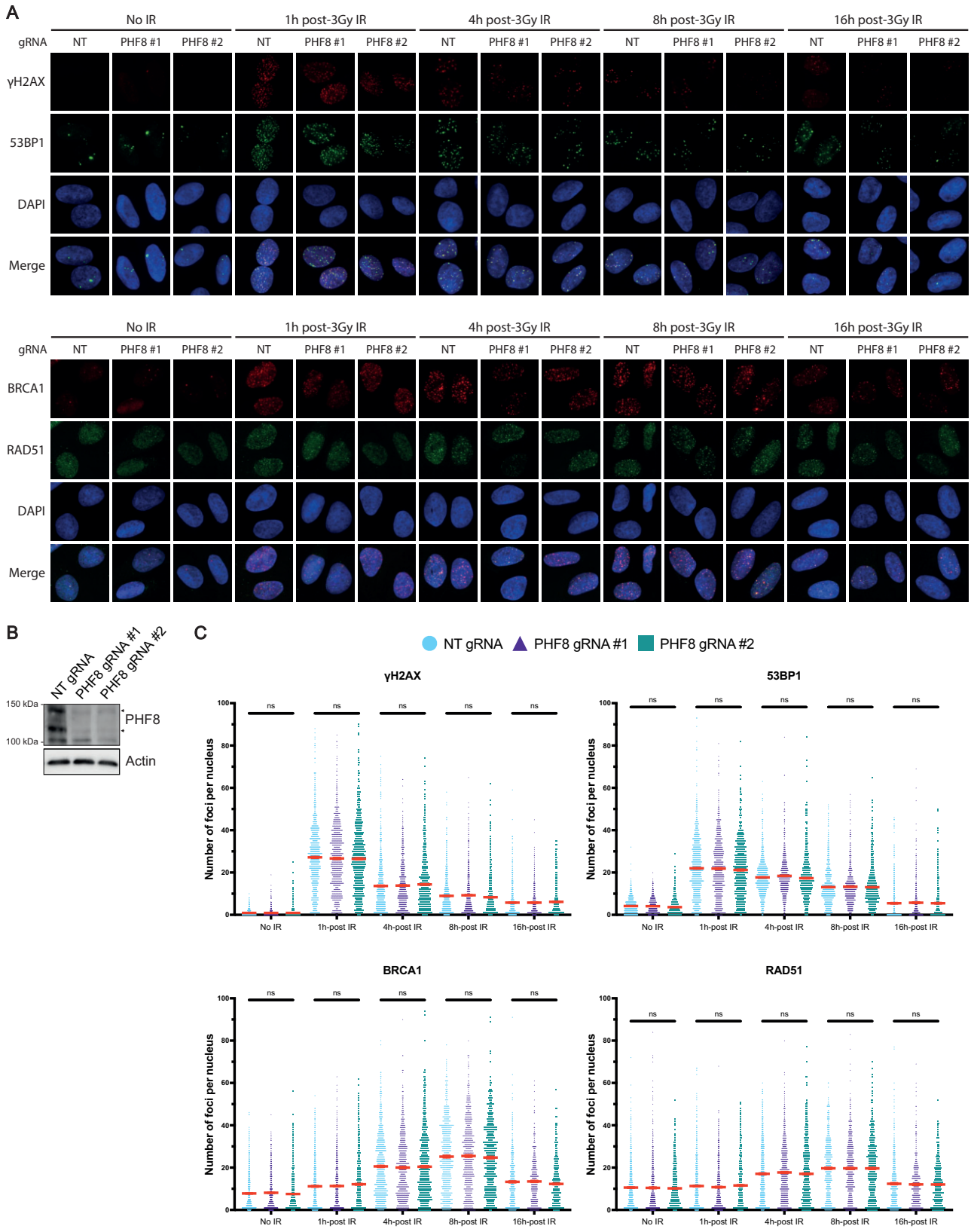

Figure 6. PHF8 does not appear to be important for DSB repair. (**A**) U2OS cells transduced with NT gRNA or PHF8 gRNA #1 or #2 were exposed to 3 Gy ionizing radiation (IR). Cells were fixed after 1, 4, 8 and 16 h and processed for immunofluorescence with anti-γH2AX and anti-53BP1 or anti-BRCA1 and anti-RAD51 antibodies. (**B**) Western blotting was performed to evaluate PHF8 expression. Arrows denote the bands of endogenous PHF8. (**C**) The number of respective foci per nucleus was analysed. Bars represent mean ± SEM; ns, non-significant.

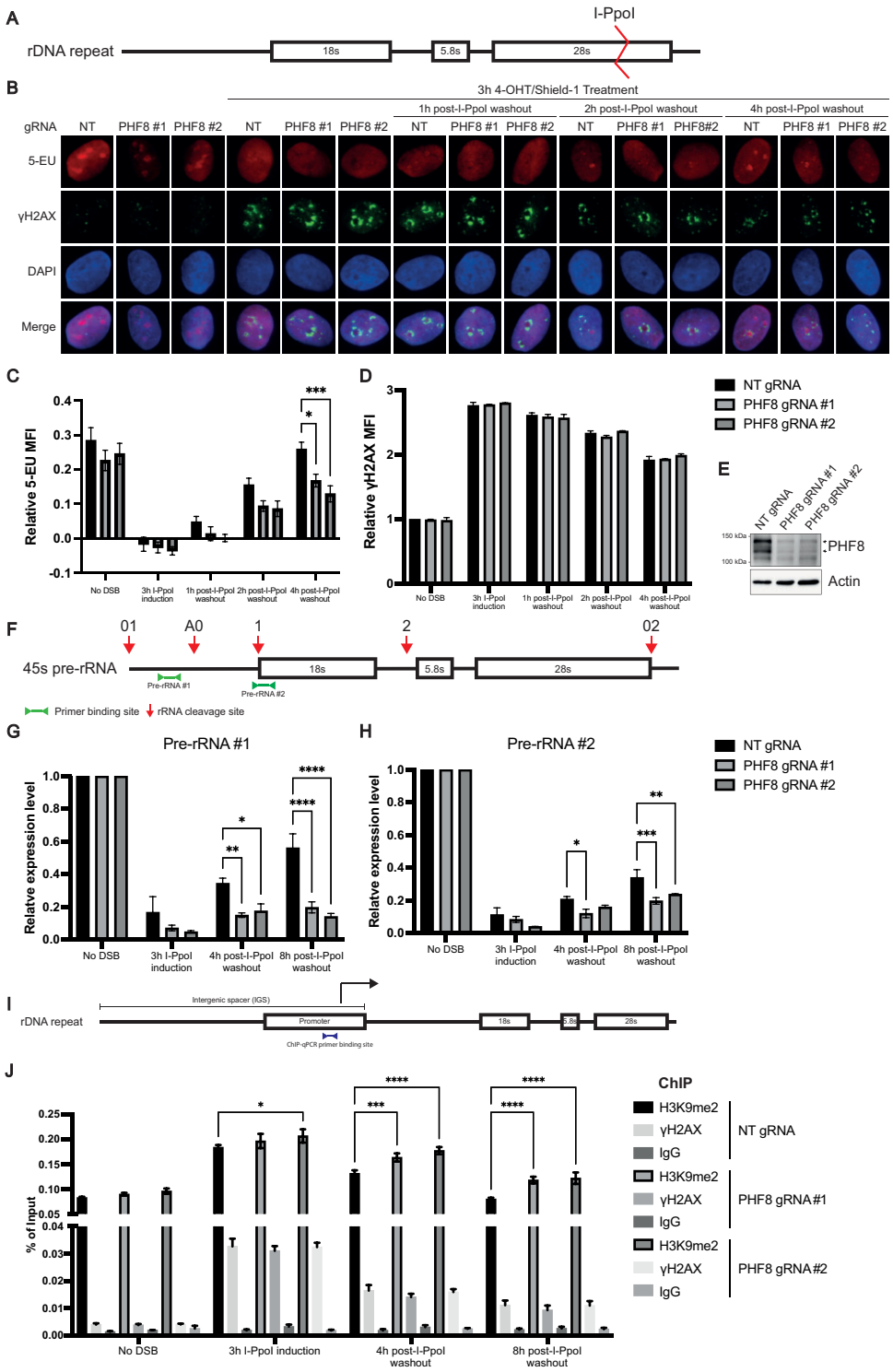

Figure 7. PHF8 promotes transcription recovery during rDNA DSB repair. (**A**) Schematic diagram represents a transcribed region of 45S ribosomal DNA (rDNA) repeats and the I-PpoI target site. (**B**) U2OS I-PpoI cells transduced with NT gRNA or PHF8 gRNA #1 or #2 were treated with 4-OHT and Shield-1 for 3 h to generate rDNA DSBs by I-PpoI. Afterwards, cells were washed with PBS and incubated for an additional 1, 2 and 4 h. To analyse the transcription activity at the nucleolus, cells were cultured in a medium supplemented with 5-EU for 1 h before fixation. Cells were labelled with 5-EU and H2AX. (**C**) Quantification shows the relative 5-EU nucleolar mean fluorescence intensity. Bars represent mean ± SEM; $*P < 0.05$; $***P \leq 0.001$. (**D**) Quantification of relative γH2AX MFI. Bars represent mean ± SEM. (**E**) Western blotting was performed to evaluate PHF8 expression. Arrows denote the bands of endogenous PHF8. (**F**) Schematic diagram shows 45S ribosomal RNA (rRNA). Green arrows denote the RT-qPCR primer binding sites. Red arrows denote the pre-rRNA cleavage site for rRNA processing. (G-H) RT-qPCR analysis of the pre-rRNA level in NT gRNA and PHF8 gRNA #1 or #2 transduced cells. Each cell group's data were normalized to its own No DSB treatment group, respectively. Bars represent mean ± SEM; $*P < 0.05$; $**P \leq 0.01$; $***P \leq 0.001$; $****P \leq 0.0001$. (**I**) Schematic diagram represents a 45S ribosomal DNA (rDNA) repeat, including a non-transcribed intergenic spacer with promoter region. Blue arrow denotes the ChIP-qPCR primer binding site. (**J**) ChIP-qPCR results show enrichment of H3K9me2 and γH2AX at different time points in cells transduced with NT gRNA or PHF8 gRNA #1 or #2. IgG was used as a negative control for ChIP. Bars represent mean ± SEM; $*P < 0.05$; $**P \leq 0.01$; $***P \leq 0.001$; $****P \leq 0.0001$.

during cell recovery from DSBs. Noting that the HR and NHEJ reporters rely on the relative expression of GFP, which is dependent on transcription activity, one may speculate that the GFP-based assays may have been confounded by a role of PHF8 in transcription regulation rather than its direct involvement in the DNA repair process. Alternatively, it also remains plausible that PHF8 may specifically promote DSB repair on specialized chromatin domains. Further studies employing additional methodologies are necessary to delineate the distinct functions of PHF8 in DNA repair and transcription regulation. Similarly, in contrast to the finding where cell pre-treatment with the H3K9-specific inhibitor UNC0638 partially and indirectly, via HP1, attenuated focal accumulation of BRCA1–BARD1 1 h post-IR (23), we found that PHF8 inactivation did not noticeably affect BRCA1 foci formation over a 16-h time course. Given the proposition that the BRCA1–BARD1 complex assembles at IR-induced DSBs via an RNF168-independent manner, one would speculate that H3K9me2 does not play a direct role in the H2AX–RNF8–RNF168-dependent pathway that is important in the maturation of DNA damage foci (24).

Our observation that early recruitment of PHF8 to DSBs is not dependent on EHMT2 activity (Figure 2C and D) suggests that its ability to enrich on the damaged chromatin may not be driven by the H3K9me2 mark, but possibly by other protein-protein interactions, including DYRK1B (Supplementary Figure S1B). Moreover, that the inactivation of PHF8 demethylase activity partially compromised its accrual to laser-induced DNA damage tracks lends credence to the idea that PHF8 may dock at DSBs via multiple protein–protein interactions.

We also documented the role of PHF8 in resuming rDNA transcription following DSBs on the rDNA locus. The proper functioning of rRNAs is essential for protein synthesis, a fundamental process for cellular function. The capacity of PHF8 to reinstate and maintain transcriptome signatures, including rDNA transcription, underlines its crucial role in the preservation of cellular function and integrity. In the absence of such restoration, cellular functions and identity could undergo profound changes, consistent with the essential role of PHF8 in maintaining proper cellular function and integrity. PHF8 variants have been associated with a range of neurodevelopmental disorders and facial dysmorphology (17,18,25–27), and noting that dysregulated ribosomal biogenesis has been linked to synaptic dysfunction and can hinder the growth and maintenance of dendrites and synapses (28,29), it would be of interest to investigate how PHF8-dependent rRNA synthesis following genotoxic stress may be associated with neurological disorders. Moreover, that PHF8 inactivation did not noticeably affect rDNA transcription in unperturbed cells (Supplementary Figure S3D–G), observations that contrast earlier reports (11,12) also warrants further investigation into how the demethylase may support rRNA synthesis and stability.

In comparison to DISC, recovery of transcription during DSB repair is an area that is largely undefined. Our finding that PHF8 plays an important role in the timely resolution of H3K9me2 and resumption of transcription is consistent with the idea that dynamic regulation of this epigenetic mark underlies the recovery of gene expression programmes. As such, further investigation of the antagonistic relationship between EHMT2 and PHF8 at the damaged chromatin throughout the DSB repair process would be of interest. Given the master role of DYRK1B in regulating the accumulation of both EHMT2 and PHF8 at DSBs, understanding the interplay between these two effectors that regulate H3K9 methylation status would be crucial. Along this line, PHF8 inactivation did not restore DISC in EHMT2-inhibited cells (Supplementary Figure S4A–C), suggesting that EHMT2-dependent H3K9me2 deposition precedes PHF8 activity. In addition, aside from PHF8, we also observed recruitment of JMJD2A to laser-induced DNA damage track, implicating its potential role in transcription resumption following DSB repair, although it appears to participate in a DYRK1B–EHMT2-independent pathway. Testing whether JMJD2A may also contribute to reversing DISC and affect the dynamic regulation of H3K9me2 on damaged chromatin would provide additional perspectives into this complex process.

In summary, this study provides important insights into the dynamics of chromatin modifications and transcriptional regulation during DSB responses. Our findings not only highlight the role of H3K9me2 in local transcription repression in response to DSBs, but also shed light on the function of PHF8 during the recovery phase of DDR, which may have far-reaching implications for understanding and treating neurological disorders associated with PHF8 mutations.

Data availability

All data are available upon request. The source of all expression constructs and antibodies is detailed in Supplementary Tables S1 and S2. Sequence of siRNAs, gRNAs and primer oligonucleotides are in Supplementary Tables S3–S6.

Supplementary data

Supplementary Data are available at NAR Online.

Acknowledgements

The authors acknowledge technical support from Centre for PanorOmic Sciences (The University of Hong Kong) and wish to thank Drs Roger Greenberg and Gaelle Legube for generous sharing of reagents.

Author contributions: J.E.K. performed all experiments and analysed results unless otherwise specified. M.S.Y.H. and J.E.K. conceptualized the work and wrote the manuscript. X.P., K.Y.W., H.H.C. and C.D. performed initial cloning and characterization of demethylases.

Funding

Research Grants Council Hong Kong [17100621, 17101223 and T12-702/20/N to M.S.Y.H.]. Funding for open access charge: Research Grants Council Hong Kong.

Conflict of interest statement

None declared.

References

1. Clouaire,T. and Legube,G. (2019) A snapshot on the *cis* chromatin response to DNA double-strand breaks. *Trends Genet.*, **35**, 330–345.

2. Tan,X.Y. and Huen,M.S.Y. (2020) Perfecting DNA double-strand break repair on transcribed chromatin. *Essays Biochem.*, **64**, 705–719.
3. Capozzo,I., Iannelli,F., Francia,S. and d'Adda di Fagagna,F. (2017) Express or repress? The transcriptional dilemma of damaged chromatin. *FEBS J.*, **284**, 2133–2147.
4. Dong,C., West,K.L., Tan,X.Y., Li,J., Ishibashi,T., Yu,C.H., Sy,S.M.H., Leung,J.W.C. and Huen,M.S.Y. (2020) Screen identifies DYRK1B network as mediator of transcription repression on damaged chromatin. *Proc. Natl Acad. Sci. U.S.A.*, **117**, 17019–17030.
5. Dong,C., An,L., Yu,C.H. and Huen,M.S.Y. (2021) A DYRK1B-dependent pathway suppresses rDNA transcription in response to DNA damage. *Nucleic Acids Res.*, **49**, 1485–1496.
6. Shanbhag,N.M., Rafalska-Metcalf,I.U., Balane-Bolivar,C., Janicki,S.M. and Greenberg,R.A. (2010) ATM-dependent chromatin changes silence transcription *in cis* to DNA double-strand breaks. *Cell*, **141**, 970–981.
7. Shinkai,Y. and Tachibana,M. (2011) H3K9 methyltransferase G9a and the related molecule GLP. *Genes Dev.*, **25**, 781–788.
8. Tachibana,M., Ueda,J., Fukuda,M., Takeda,N., Ohta,T., Iwanari,H., Sakihama,T., Kodama,T., Hamakubo,T. and Shinkai,Y. (2005) Histone methyltransferases G9a and GLP form heteromeric complexes and are both crucial for methylation of euchromatin at H3-K9. *Genes Dev.*, **19**, 815–826.
9. Wang,Z., Zang,C., Rosenfeld,J.A., Schones,D.E., Barski,A., Cuddapah,S., Cui,K., Roh,T.Y., Peng,W., Zhang,M.Q., *et al.* (2008) Combinatorial patterns of histone acetylations and methylations in the human genome. *Nat. Genet.*, **40**, 897–903.
10. Hunt,C.R., Ramnarain,D., Horikoshi,N., Iyengar,P., Pandita,R.K., Shay,J.W. and Pandita,T.K. (2013) Histone modifications and DNA double-strand break repair after exposure to ionizing radiations. *Radiat. Res.*, **179**, 383–392.
11. Feng,W., Yonezawa,M., Ye,J., Jenuwein,T. and Grummt,I. (2010) PHF8 activates transcription of rRNA genes through H3K4me3 binding and H3K9me1/2 demethylation. *Nat. Struct. Mol. Biol.*, **17**, 445–450.
12. Zhu,Z., Wang,Y., Li,X., Wang,Y., Xu,L., Wang,X., Sun,T., Dong,X., Chen,L., Mao,H., *et al.* (2010) PHF8 is a histone H3K9me2 demethylase regulating rRNA synthesis. *Cell Res.*, **20**, 794–801.
13. Tsukada,Y., Fang,J., Erdjument-Bromage,H., Warren,M.E., Borchers,C.H., Tempst,P. and Zhang,Y. (2006) Histone demethylation by a family of JmjC domain-containing proteins. *Nature*, **439**, 811–816.
14. Yamane,K., Toumazou,C., Tsukada,Y., Erdjument-Bromage,H., Tempst,P., Wong,J. and Zhang,Y. (2006) JHDM2A, a JmjC-containing H3K9 demethylase, facilitates transcription activation by androgen receptor. *Cell*, **125**, 483–495.
15. Couture,J.F., Collazo,E., Ortiz-Tello,P.A., Brunzelle,J.S. and Trievel,R.C. (2007) Specificity and mechanism of JMJD2A, a trimethyllysine-specific histone demethylase. *Nat. Struct. Mol. Biol.*, **14**, 689–695.
16. Whetstine,J.R., Nottke,A., Lan,F., Huarte,M., Smolikov,S., Chen,Z., Spooner,E., Li,E., Zhang,G., Colaiacovo,M., *et al.* (2006) Reversal of histone lysine trimethylation by the JMJD2 family of histone demethylases. *Cell*, **125**, 467–481.
17. Laumonnier,F., Holbert,S., Ronce,N., Faravelli,F., Lenzner,S., Schwartz,C.E., Lespinasse,J., Van Esch,H., Lacombe,D., Goizet,C., *et al.* (2005) Mutations in PHF8 are associated with X linked mental retardation and cleft lip/cleft palate. *J. Med. Genet.*, **42**, 780–786.
18. Abidi,F., Miano,M., Murray,J. and Schwartz,C. (2007) A novel mutation in the PHF8 gene is associated with X-linked mental retardation with cleft lip/cleft palate. *Clin. Genet.*, **72**, 19–22.
19. Iacovoni,J.S., Caron,P., Lassadi,I., Nicolas,E., Massip,L., Trouche,D. and Legube,G. (2010) High-resolution profiling of gammaH2AX around DNA double strand breaks in the mammalian genome. *EMBO J.*, **29**, 1446–1457.
20. Iannelli,F., Galbiati,A., Capozzo,I., Nguyen,Q., Magnuson,B., Michelini,F., D'Alessandro,G., Cabrini,M., Roncador,M., Francia,S., *et al.* (2017) A damaged genome's transcriptional landscape through multilayered expression profiling around *in situ*-mapped DNA double-strand breaks. *Nat. Commun.*, **8**, 15656.
21. Jeon,H.Y., Hussain,A. and Qi,J. (2020) Role of H3K9 demethylases in DNA double-strand break repair. *J. Cancer Biol.*, **1**, 10–15.
22. Wang,Q., Ma,S., Song,N., Li,X., Liu,L., Yang,S., Ding,X., Shan,L., Zhou,X., Su,D., *et al.* (2016) Stabilization of histone demethylase PHF8 by USP7 promotes breast carcinogenesis. *J. Clin. Invest.*, **126**, 2205–2220.
23. Wu,W., Nishikawa,H., Fukuda,T., Vittal,V., Asano,M., Miyoshi,Y., Klevit,R.E. and Ohta,T. (2015) Interaction of BARD1 and HP1 is required for BRCA1 retention at sites of DNA damage. *Cancer Res.*, **75**, 1311–1321.
24. Huen,M.S. and Chen,J. (2010) Assembly of checkpoint and repair machineries at DNA damage sites. *Trends Biochem. Sci.*, **35**, 101–108.
25. Loenarz,C., Ge,W., Coleman,M.L., Rose,N.R., Cooper,C.D., Klose,R.J., Ratcliffe,P.J. and Schofield,C.J. (2010) PHF8, a gene associated with cleft lip/palate and mental retardation, encodes for an nepsilon-dimethyl lysine demethylase. *Hum. Mol. Genet.*, **19**, 217–222.
26. Qiu,J., Shi,G., Jia,Y., Li,J., Wu,M., Li,J., Dong,S. and Wong,J. (2010) The X-linked mental retardation gene PHF8 is a histone demethylase involved in neuronal differentiation. *Cell Res.*, **20**, 908–918.
27. Chen,X., Wang,S., Zhou,Y., Han,Y., Li,S., Xu,Q., Xu,L., Zhu,Z., Deng,Y., Yu,L., *et al.* (2018) Phf8 histone demethylase deficiency causes cognitive impairments through the mTOR pathway. *Nat. Commun.*, **9**, 114.
28. Hetman,M. and Slomnicki,L.P. (2019) Ribosomal biogenesis as an emerging target of neurodevelopmental pathologies. *J. Neurochem.*, **148**, 325–347.
29. Slomnicki,L.P., Pietrzak,M., Vashishta,A., Jones,J., Lynch,N., Elliot,S., Poulos,E., Malicote,D., Morris,B.E., Hallgren,J., *et al.* (2016) Requirement of neuronal ribosome synthesis for growth and maintenance of the dendritic tree. *J. Biol. Chem.*, **291**, 5721–5739.

Received: November 13, 2023. **Revised:** July 11, 2024. **Editorial Decision:** July 17, 2024. **Accepted:** July 18, 2024